Astrocyte Molecular Clock Function in the Nucleus Accumbens Is Important for Reward-Related Behavior

Supplemental Information

Supplementary Methods

Animals

Behavioral and molecular experiments utilized male and female *Bmal1* "floxed" (BMFL) mutant mice, ages 10-14 weeks old (*Bmal1*^{lox}, B6.129S4-Arntltm1Weit/J; Stock No: 007668, The Jackson Laboratory; Bar Harbor, ME). When Cre recombinase is expressed in BMFL mice, the exon encoding BMAL1's basic helix-loop-helix (bHLH) functional domain is deleted, resulting in loss of circadian clock regulated rhythmicity (1). Rhythmicity characterization experiments utilized male and female Aldh1l1-eGFP/Rpl10a (B6;FVB-Tg(Aldh1l1-EGFP/Rpl10a)JD133Htz/J; JAX Stock No: 007668; RRID:IMSR_JAX:030247) expressing an eGFP fluorophore under the *Aldh1l1* promotor, an established pan-astrocyte marker (2–4). All mice were maintained on a 12:12 light-dark cycle (lights on: 0700 zeitgeber time (ZT) 0; lights off: 1900, ZT12) and provided *ad libitum* food and water access unless otherwise indicated. Animal use was conducted under guidelines set by the National Institutes of Health (NIH), and all procedures were approved by the University of Pittsburgh Institutional Animal Care and Use Committee (IACUC).

Immunoprecipitation (IP) and RNA extraction from NAc Astrocytes

NAc tissue was collected from both male and female Aldh1l1-eGFP/Rpl10a mice across 6 times of days (ZT2,6,10,14,18, & 22; 10M/8F per ZT). Immunoprecipitation of polyribosomes from Aldh1l1-eGFP/Rpl10a was processed using a modified protocol described previously (5, 6). For each sample, the NAc from 2 mice were pooled and homogenized in a Dounce homogenizer with a buffer containing 50 mM Tris-HCl, 100 mM KCl, 12 mM MgCl2, and 1% NP-40, supplemented with 1 mM DTT, 100 µg/ml cycloheximide (Sigma-Aldrich; St. Louis, MO), RNasin® Plus ribonuclease inhibitor (Promega; Madison, WI), and EDTA-free protein inhibitor cocktail (Roche; Basel, CH; cat# 11873580001 Following a 10 minute 10,000g centrifugation step, the supernatant was transferred to low-protein binding tubes and mixed with 20 µg of anti-GFP antibody (ab290; Abcam; Cambridge, UK; RRID:AB_303395), rotating overnight at 4°C. The following day, 12 mg of Dynabeads Protein G (Invitrogen; cat#10009D) were washed once in non-supplemented homogenization buffer and then added to antibody-bound lysate samples for an additional overnight incubation step at 4°C. Finally, beads were washed 3 times in a high salt buffer containing 50 mM Tris-HCl, 300 mM KCl, 12 mM MgCl2, 1% NP-40, 1 mM DTT, and 100 µg/ml cycloheximide. Elution of polyribosomes from beads was performed in TRK lysis buffer + β-ME provided in the Omega Micro Elute Total RNA kit (Omega Bio-Tek; Norcross, GA). The supernatant was removed from beads using the DynaMag-2 magnetic rack (Invitrogen) and then processed for RNA following the kit provided manufacturer instructions. Final eluted NAc astrocyte-specific RNA was used for RNA-sequencing.

Library preparation and next-generation RNA sequencing

Prior to library preparation, isolated RNA samples were quantified by fluorometry using the Qubit RNA High Sensitivity assay (Qubit 4 Fluorometer; Invitrogen; Carlsbad, CA; cat# Q32852; RRID:SCR_018095) and assessed for quality/integrity with chromatography using the Agilent RNA 6000 Pico Kit (2100 Bioanalyzer; Agilent, Santa Clara, CA; cat# 5067-1513; RRID:SCR_018043). Across the 54 pooled samples, the average RNA integrity number (RIN) was ~7, with an average concentration of ~18 ng/µl. Library preparation was performed with >100 ng of RNA from each sample using the TruSeq Stranded Total RNA Kit (Illumina; San Diego, CA; cat# 20020599), as per the manufacturer's instructions. Briefly, Total RNA input was depleted for rRNA and fragmented. Random primers initiated first and second-strand cDNA synthesis. Adenylation of 3' ends was followed by adapter ligation and library amplification with indexing. One sample from ZT 14 did not generate a library and was therefore excluded. Single-read 75bp sequencing at 40 million reads per sample was performed using the Illumina NextSeq 500 platform through the University of Pittsburgh Health Sciences Sequencing Core at UPMC Children's Hospital of Pittsburgh.

RNA sequencing analysis: Pre-Processing & Rhythmicity Detection

Pre-Processing. FastQC v0.11.7 (https://bioinformatics.babraham.ac.uk/projects/fastqc/; RRID:SCR_014583) was performed to assess the quality of the data. Per base sequence quality was high (Quality score generally > 30), indicating good data quality. HISAT2 (HISAT2 v2.1; RRID:SCR_015530) was then used to align reads to the reference genome (Mus musculus Ensembl GRCm38 – mm10) using default parameters (7). The resulting bam files were converted

to expression count data using HTSeq (HTSeq v0.10) with default union mode (8). One sample from ZT 18 was removed due to its consistently low expression. RNA-seq count data were transformed to log2 continuous counts per million (cpm) data using the cpm function of the Bioconductor edgeR package (RRID:SCR_012802) (9, 10). Genes were retained for analysis if log2(cpm) was >1 in 50% or more of samples. All Y-chromosome genes were also removed from the analysis. After filtering, 12,739 genes remained for further analysis.

Rhythmicity Detection. Across the 54 pooled samples (9 samples per 6 ZT), the JTK_CYCLE package for R was used to detect circadian rhythmicity of NAc astrocyte-specific genes, with parameters set to 22-26hr to fit time-series data to periodic waveforms (RRID:SCR_017962) (11, 12). The JTK_Cycle statistical algorithm utilizes a non-parametric harmonic regression / sinusoidal fit test to output both a Bonferonni-Adjusted p-value (Adj.P) and a Benjami-Hochberg q-value (BH.Q), distinguishing between rhythmic and non-rhythmic transcripts. This algorithm also assesses other circadian parameters, including period, phase, and amplitude. From the 12,739 genes, 5527 transcripts were determined to rhythmic at the $p<0.05$ Adj.P cutoff, and 1,131 transcripts at the more statistically rigorous BH.Q cutoff. A heatmap of the top 200 circadian transcripts was generated using the gplots R package (v.3.1), where the expression levels for each top gene were Z-transformed, ordered on the y-axis descending by significance, and each column along the x-axis representing a sample ordered by phase (i.e., ZT). A radar plot of phase distribution across all rhythmic transcripts ($p<0.05$; 5,527) was created using DisplayR online data analysis and visualization software (https://www.displayr.com/).

Rank-rank hypergeometric overlap (RRHO). RRHO was used as a threshold-free analysis to identify overlap between two genes lists (13, 14). In this analysis, genes are ranked by their −log10(p value) and effect size direction, and a heat map is generated to identify significantly

overlapping genes across a continuous significance gradient rather than at a single arbitrary cut-off. We used RRHO to evaluate the degree of similarity/overlap between JTK_Cycle detected rhythmic transcripts in males versus females.

Enriched Pathways and Biological Processes Analysis

Both Ingenuity Pathway Analysis (IPA) software (QIAGEN; Hilden, Germany; RRID:SCR_008653) (15) and the online bioinformatics database Metascape (https://metascape.org/; RRID:SCR_016620) (16) were used to identify enriched molecular pathways and processes in both the top enriched (200 genes with highest Log2CPM) and top rhythmic (BH $q<0.0001$) gene lists. For both analyses, gene lists were analyzed as follows: (1) after filtering, the remaining 12,739 annotated genes were used as the background/reference gene list; (2) the lists of top 200 enriched genes (highest Log2CPM) and 1,141 top rhythmic genes ($q<0.0001$) were used as input lists for both IPA and Metascape analyses; and (3) for identification of significant pathways and processes, a significance threshold of $p<0.05$ (or a -log10(p-value) of 1.3 in figures) was utilized. IPA software was used to identify enriched canonical molecular pathways, while Metascape was used to identify enriched biological processes using only *Gene Ontology (GO) Biological Processes* as the ontology source. Within Metascape, all statistically enriched terms, accumulative hypergeometric p-values, and enrichment factors were automatically calculated and used for filtering. The remaining significant terms were then hierarchically clustered into a tree based on Kappa-statistical similarities among their gene memberships, with a 0.3 kappa score applied as the threshold to cast the tree into term clusters. The most significant term in each cluster served as the cluster title. Process enrichment was detected using the default

settings of a p<0.01 cutoff, minimum overlap of 3, and a minimum enrichment of 1.5. A subset of representative terms from this cluster were then converted into an enrichment network using Cytoscape (v3.1.2; RRID:SCR_003032) (17), with each term represented by a circle node colored by cluster identity and terms with a similarity score > 0.3 linked together (the thickness representing the similarity score). (16)

RNAscope® in situ hybridization (ISH)

For qualitative validation of Aldh1l1-eGFP/Rpl10a mice, the RNAscope in situ hybridization (ISH) Fluorescent Multiplex Assay (cat# 320850; Advanced Cell Diagnostics; Newark, CA) was utilized. First, brains were rapidly removed, flash-frozen, and stored at -80C until further processing. Brains were then cryo-sectioned at 14 microns to isolate NAc containing sections, mounted on slides, and processed using the RNAscope Fluorescent Multiplex kit following the company-provided protocol. Briefly, mounted tissue sections were fixed in 4°C chilled 10% normal buffered formalin for 30 minutes, followed by 1xPBS washing and a series of ethanol dehydration steps (50,70, & 100% EtOH) at room temperature. Following the addition of an ImmEdge® hydrophobic barrier (Vector Labs; Burlingame, CA; RRID:AB_2336517), tissue sections were then hybridized with catalog probes against *Aldh1l1*, *eGFP*, and *Slc32a1* (ACD cat#405891, #400281-c3, & #319191-c2, respectively) at 40°C for 2 hours in the ACD HybEZ™ Hybridization Oven (Cat#310010). Amplification of signal was performed through 40°C incubation with sequential amplifiers AMP1-3 and AMP4 Alt-C was used to detect *Aldh1l1* in Atto 550, *eGFP* in Alexa 488, and *Slc32a1* (i.e., *Vgat*) in Atto 647. Sections were washed in the kit provided 1x wash buffer before being counterstained with DAPI and cover-slipped with ProLong™ Gold Antifade Mountant (#P36930; Invitrogen; Carlsbad, CA). Slides were stored at

4°C overnight protected from light before imaging using an Olympus Fluoview FV1200 confocal microscope (Olympus Corporation; Shinjuku, Tokyo, Japan). Images of the NAc were captured sequentially by frame at 60x magnification with 5-6 x 2.2 µm z-stacks, an 8.0 µs/pixel sampling speed, and 1024 x 1024 (pixel) image dimension. For representative images, the z-axis was collapsed into a single plane to show all signal across channels. Images were formatted using Olympus Fluoview FV10-ASW 4.2 viewer software (Olympus; RRID:SCR_014215).

Viral-Placement Surgery and Verification

BMFL mice were injected at 8 weeks of age with either AAV8-GFAP-eGFP or AAV8-GFAP-Cre-GFP viral vectors (UNC Viral Vector Core; Chapel Hill, NC; RRID:SCR_002448) into the NAc following protocols previously published (18). Briefly, male and female BMFL mice under isoflurane anesthesia were given bilateral stereotaxic 1 µl injections into the NAc (Bregma: AP +1.5, ML ±1.5, DV -4.4 mm; angle 10°) of respective purified high titer adeno-associated virus. To allow for sufficient viral expression, mice were allowed at least 2 weeks to recover before starting behaviors or collecting tissue for subsequent molecular assays. Expression of Cre recombinase in the NAc under the *Gfap* promoter induces a functional ablation of BMAL1 specifically in astrocytes and results in loss of astrocyte rhythmicity, as previously demonstrated and validated (19, 20). Viral placement, spread, and specificity were verified qualitatively using immunofluorescence (IF). In short, mice were perfused with 4% paraformaldehyde (PFA) in phosphate-buffered saline (PBS) at pH 7.4, and brains were isolated for post-fixation plus 30% sucrose saturation. Brains were then cryo-sectioned at 40 microns before processing for IF. Green Fluorescent Protein (GFP) signal was enhanced using a primary anti-GFP antibody (ab13970; Abcam, Cambridge, UK; RRID:AB_300798), and specificity was verified against anti-BMAL1

(NB100-2288; Novus Biologicals; Centennial, CO; RRID:AB_10000794) or anti-GFAP (NBP1-05197; Novus; RRID:AB_1555288), as previously validated (19). Sections were mounted on slides with VECTASHIELD mounting medium plus DAPI (Vector Laboratories; Burlingame, CA, USA; RRID:AB_2336788). Sections were imaged at 10x and 20x magnification using an Olympus Fluoview FV1200 confocal microscope (Olympus Corporation; Shinjuku, Tokyo, Japan). Images were formatted using Olympus Fluoview FV10-ASW 4.2 viewer software (Olympus; RRID:SCR_014215).

Behavioral Testing

A battery of behavioral tests assessing reward-related behaviors was conducted with both BMFL-NAc: GFAP-Cre mice and eGFP control mice. Behavioral testing was conducted between ZT2-6 or ZT 14-18, with at least 30 minutes of habituation to the room before testing. Following testing, mice were returned to their home cage for at least 48 hours before moving on to the next behavioral assay.

Locomotor Response to Novelty (LRN). Mice were placed individually in 25 x 45 cm plexiglass boxes equipped with photo beams (Kinder Scientific Smart Cage Rack System; Poway, CA). Distance traveled (cm) was recorded for 2 hours in 5-minute bins, as well as overall total distance.

Open Field (OF). Under 20 lux lighting, mice were placed individually in a large black plexiglass arena (52 x 52 x 25 cm) and allowed to explore for 10 min freely. Behavior was recorded and analyzed using Ethovision XT 13 (Noldus Information Tech; Leesburg, VA; RRID:SCR_000441), calibrated by blind hand scoring. Time spent in the center of the arena (24 x 24 cm square in the center), center entries, and distance traveled were recorded.

Light / Dark Box (L/D). Mice were placed individually in a 25 x 45 cm plexiglass arena equipped with photo beams, divided into two equally sized chambers (Kinder Scientific Smart Cage Rack System; Poway, CA) – one side brightly lit (~880 lux) and the other containing a black opaque box. Mice were placed on the dark side for 2 min before a door opened, allowing mice to explore both sides for 20 minutes freely. Distance traveled, light entries, and time spent in the light side were all recorded.

Elevated Plus Maze (EPM). Under 20 lux lighting, mice were placed in the center of an elevated plus maze (81 cm off the ground), consisting of 2 open arms and 2 enclosed arms oriented perpendicularly (each 30 x 5 cm). Mice started facing an open arm and were allowed to explore the maze for 10 minutes freely. Behavior was recorded and analyzed using Ethovision XT 13, calibrated by blind hand scoring. Arm entries (both open and closed), time spent in the open arm, and distance traveled were recorded.

Novelty Suppressed Feeding (NSF). Mice were food deprived exactly 24 hours before the start of the NSF task. On test day, were placed individually in the corner of a brightly lit (700-800 lux) large black plexiglass arena (52 x 52 x 25 cm) filled with fresh bedding and a pellet of fresh food placed in the center of the arena. The mouse was allowed to explore the arena for 12 minutes *or* until the mouse takes a bite of the food. Following test completion, the mouse was returned individually to its home cage and allowed free access to 1 pellet of food for 8 minutes. Latency to eat was recorded during the test by a blind-trained scorer. Post-test food consumption (grams) and total weight loss were recorded as controls for any potential feeding differences.

Operant Food Self-Administration (Food SA). Mice were initially food-restricted overnight and then maintained at 85-90% free-feeding weight throughout the behavior. For all operant testing, mice were placed individually in an operant conditioning chamber equipped with a pellet

dispenser, a food trough with 2 levers on either side, a cue light above each lever, and an overhead chamber light (Med Associates Inc; Fairfax, VT). To test food self-administration, mice were first trained on a fixed ratio (FR) 1 schedule (1 press = 1 pellet) in daily 1-hour sessions or until mice consumed 30 pellets (chocolate-flavored 20 mg, grain-based precision pellets; Bio-Serv; Flemington, NJ). During the session, the overhead chamber light and active lever cue light were continuously lit until the end of the session. Mice were considered to have achieved acquisition criteria if they reached ≥ 25 pellets for 3 sessions in a row. After 7 sessions of food self-administration testing, motivation was then tested by increasing mice to FR3 for 3 sessions, FR5 for 2 sessions, and then FR10 for 2 sessions. All data was collected through the Med-PC software suite (Med Associates; RRID:SCR_012156). Mice were returned to free-feeding weight following operant training.

RNA isolation and RT-qPCR for Gene Expression

BMFL-NAc: GFAP-Cre and eGFP control mice were sacrificed and the NAc was quickly micro-dissected before being snap-frozen on dry ice. Total RNA was isolated using the RNeasy Plus Mini Kit (Qiagen; Hilden, Germany; cat# 74134) with QIAshredder homogenization columns (Qiagen; cat# 79656), and 100ng was converted to complementary DNA (cDNA) using the iScript cDNA synthesis kit (Bio-Rad; Hercules, CA; cat# 1708891). Quantitative polymerase chain reaction (qPCR) was then used to measure gene expression of astrocyte, metabolic, and glutamate related genes of interest. Briefly, 1 ng of cDNA was mixed with SsoAdvanced Universal SYBR Green Supermix (Bio-Rad; Hercules, CA, USA; cat# 1725272) and both forward and reverse primers. Samples were run in triplicate in a 96-well plate, performed using a CFX96 Touch Real-Time PCR detection system (Bio-Rad). The following primers were utilized (**Table S1)**:

Table S1. Astrocyte, Metabolic, and Glutamate Gene Expression Mouse Primers

Primer	Forward (5' – 3')	Reverse (5' – 3')	Ref.
18s	ACCGCAGCTAGGAATAATGGA	GCCTCAGTTCCGAAAACCA	(18)
Aldh1l1	CCAGCCTCCCAGTTCTTCAA	GGACATTGGGCAGAATTCGC	(21)
Gfap	GAAACCAACCTGAGGCTGGA	CCACATCCATCTCCACGTGG	(21)
Nrf2	TTCTTTCAGCAGCATCCTCTCCAC	ACAGCCTTCAATAGTCCCGTCCAG	(22)
Pgc1a	TCACACCAAACCCACAGAAA	TCTGGGGTCAGAGGAAGAGA	(23)
Gclc	ACATCTACCACGCAGTCAAGGACC	CTCAAGAACATCGCCTCCATTCAG	(22)
Ldha	AGGTTACACATCCTGGGCCATT	TCAGGAGTCAGTGTCACCTTCACA	(24)
Mct1	CATTGGTGTTATTGGAGGTC	GAAAGCCTGATTAAGTGGAG	(25)
Mct2	CACCACCTCCAGTCAGATCG	CTCCCACTATCACCACAGGC;	(25)
Gria1	ACTCAAGCGTCCAGAATAGAAC	AATCTCAAGTCGGTAGGAATAGC	(26)
Gria2	CAGATTGTAGACTACGACGACTC	TCATCACTTGGACAGCATCATAA	(26)
Gria3	GGTCATTCTCACGGAGGATTC	GGTGTTCTGGTTGGTGTTGTA	(26)
Gria4	CCAGTAGAGGACAACGCAATT	TGACAGAGTGAAGGTTACAGGAA	(26)
Grin1	AGATAGTGACAATCCACCAAGAAC	ACCATTGACTGTGAACTCCTC	(26)
Grin2a	GACCAGATGCTTCAGGAGACAG	CTTGAGGCTTATGCTACGAGAGG	(26)
Grin2b	GGTGTTTAACAACTCCGTACCT	GAAACCTGGTCCACATACTCCTC	(26)
Grin2c	CGTGTGGTTAGTACCTAATCTG	TTCTGGCGTAGGCTAAGG	(26)
Grin2d	AACCGAGACTACTCCTTCAATGA	GCCATAGCGGGACCATAGA	(26)
Grin3A	GACAAAGCCCTTCTGGATTATGA	ATGTTAGAGGTCAACGGAGAGT	(26)
Grin3B	TGGTCGGGGACAAGACATTT	TCCGTGTGGAGTGGTAGGTG	(27)
Grm1	CGAGTGGAGTGACATAGAATC	TACCAGCCAGAATGATATAGCA	(26)
Grm2	GCTTAGGTTCCTGGCACT	TTAACAGGTCCACACTCCTC	(28)
Grm3	CGACCACATATTCTCAGTCCTCT	AGCACTTCGTCTAACAGCCTATA	(26)
Grm4	CCCATACCCATTGTCAAGTTGG	TGTAGCGCACAAAAGTGACCA	(29)
Grm5	CAGCTTAGATCGCAGCCACT	CAAGAATTTGGGTAAAATCACCA	(26)
Glt-1	CGATGAGCCAAAGCACCGAA	CTGGAGATGATAAGAGGGAGGATG	(30)
Glast	TCAAGTTCTGCCACCCTACC	TCTGTCCAAA GTTCAGGTCAA	(30)
xCT	TGCAATCAAGCTCGTGAC	AGCTGTATAACTCCAGGGACTA	(31)

The comparative cycle threshold (ct) method (i.e., $2^{-\Delta\Delta CT}$ method) was used to calculate relative gene expression (32), normalized to the 18s reference gene. Relative gene expression values were reported as the mean normalized Ct value ± SEM.

Lactate and GSH Assays

BMFL-NAc: GFAP-Cre and eGFP control mice were sacrificed across 2 times of day (ZT5 & ZT17) and the NAc was quickly micro-dissected before being snap-frozen on dry ice. NAc tissue was then used to measure levels of both L(+)-Lactate and glutathione (GSH) utilizing established and validated colorimetric and luminescent assays (33–36). For measurement of NAc lactate concentration, 75 µg supernatant from homogenized NAc tissue was processed through the BioVision Lactate Colorimetric/Fluorometric Assay (BioVision; Milpitas, CA), as per the supplied manufacturer instructions. Samples were run in triplicate in a clear 96-well plate using an Epoch microplate spectrophotometer (BioTek; Winooski, VT). In this assay, sample lactate is the substrate for an enzyme mix that generates a product, which then reacts with a probe to produce a color detected by measuring absorbance (OD 570 nm). Lactate concentrations were calculated using a standard curve and manufacturer-provided formula. For measurement of NAc GSH concentration, 75 µg of supernatant from homogenized NAc tissue (pre-treated with 2mM EDTA and 1mg/ml heparin) was processed through the GSH-Glo™ Glutathione Luminescence Assay (Promega; Madison, WI), as per manufacturer instructions. Samples were run in triplicate in an opaque 96-well plate using an FLx800 fluorescence-luminescence microplate reader (BioTek; Winooski, VT). In this assay, a luciferin derivative is converted to luciferin in the presence of sample GSH, catalyzed by glutathione-S-transferase. The luciferin generated is the substrate for luciferase, whereby the light generated is directly proportional to the amount of GSH. GSH concentrations were calculated using a standard curve. For both lactate and GSH, levels are reported as concentrations (nmol) divided by the input (µg).

Electrophysiology Recordings

Whole-cell patch-clamp recordings were conducted using NAc-containing sections from both BMFL-NAc: GFAP-Cre and eGFP control mice. Recordings were conducted during the light phase (ZT4-6) and the dark phase (ZT16-18). Briefly, mice were deeply anesthetized with isoflurane and decapitated. The brain was removed and placed in an ice-cold, oxygenated cutting solution made of (in mM): 135 *N*-methyl-D-glucamine, 1 KCl, 1.2 KH_2PO_4, 1.5 $MgCl_2$, 0.5 $CaCl_2$, 20 choline bicarbonate, and 10 D-glucose (pH 7.4, adjusted with HCl). Sections (250 µm) were cut on a vibratome (Leica VT1200S; Leica Biosystems; Wetzlar, Germany) and placed into oxygenated aCSF containing (in mM): 119 NaCl, 2.5 KCl, 1 NaH_2PO_4, 26.2 $NaHCO_3$, 1.3 $MgCl_2$, 2.5 $CaCl_2$, and 11 D-glucose, at 37ºC briefly before returning to room temperature before recordings.

For recordings, sections were perfused with heated oxygenated aCSF containing 100 µM picrotoxin (Tocris) (~29-31°C). The NAc was identified at 5x, GFP expressing cells were visualized using a 488 nm fluorescence filter set, and neighboring presumptive MSNs for recordings were identified at 40x under differential interference contrast (Leica). Borosilicate glass recording pipettes (~3-4.5MΩ) were filled with an internal saline solution containing (in mM): 108 $CsMeSO_3$, 15 CsCl, 0.4 Cs-EGTA, 5 TEA-Cl, 20 HEPES, 2.5 Mg-ATP, 0.25 Na-GTP, 1 QX-314, and 7.5 phosphocreatine (pH 7.3, adjusted with CsOH). Excitatory postsynaptic currents (EPSCs) were evoked with a monopolar electrode filled with bath aCSF (without picrotoxin) using a constant-current isolated stimulator (50 µA, 0.1 ms) (DS3, Digitimer). To determine AMPA/NMDA ratio, AMPAR current was measured as the peak amplitude at -70mV below the AMPA-NMDA reversal potential. NMDAR amplitude was measured at +40 mV above the AMPA-NMDA reversal potential and operationally defined as the amplitude at 35 ms following

the AMPAR EPSC peak (37). Recordings with >20% change in series resistance were excluded from the analysis. High-frequency stimulation trains contain 5 of 0.1 ms pulses delivered at 50 Hz.

All recordings were made with a MultiClamp 700A amplifier (Molecular Devices; San Jose, CA), filtered at 2 kHz, amplified 5 times, and digitized at 20 kHz using a Digidata 1322 analog-to-digital converter (Molecular Devices). Analysis was performed using pClamp 11 (Molecular Devices; RRID:SCR_011323). Exclusion criteria for all experiments included: poor access, inability to detect viral eGFP expression using the standard camera and microscope settings, and/or if the data point exceeded two times the standard deviation of the mean.

Statistical Analyses

GraphPad Prism 9 software (GraphPad Software; San Diego, CA, USA; RRID:SCR_002798) was utilized for all statistical data analyses. For statistical analysis of more than two groups, one-way, two-way, or three-way analysis of variance (ANOVA) was utilized with significant interactions followed by Bonferroni *post-hoc* tests corrected for multiple comparisons. Repeated measures were employed where appropriate. Statistical analysis of two groups was performed using a Student's t-test. Across all data sets, outliers were tested for using the Grubbs' test ($\alpha = 0.05$), and no more than 1 outlier was removed if it exceeded the critical value of Z. Statistical analyses tested for sex as a variable; throughout, males and females are grouped together unless a main effect of sex was detected, in which case males and females are displayed separately. Z-normalization (i.e., Z-scoring) of behavioral data from exploratory drive assays was performed as published (38), whereby relevant parameters from each of the assays were converted to Z-scores, indicating how many standard deviations the observations were above or below the

control mean. Unless otherwise noted, all data are shown as mean ± SEM with $\alpha = 0.05$ considered statistically significant.

Supplemental Figures

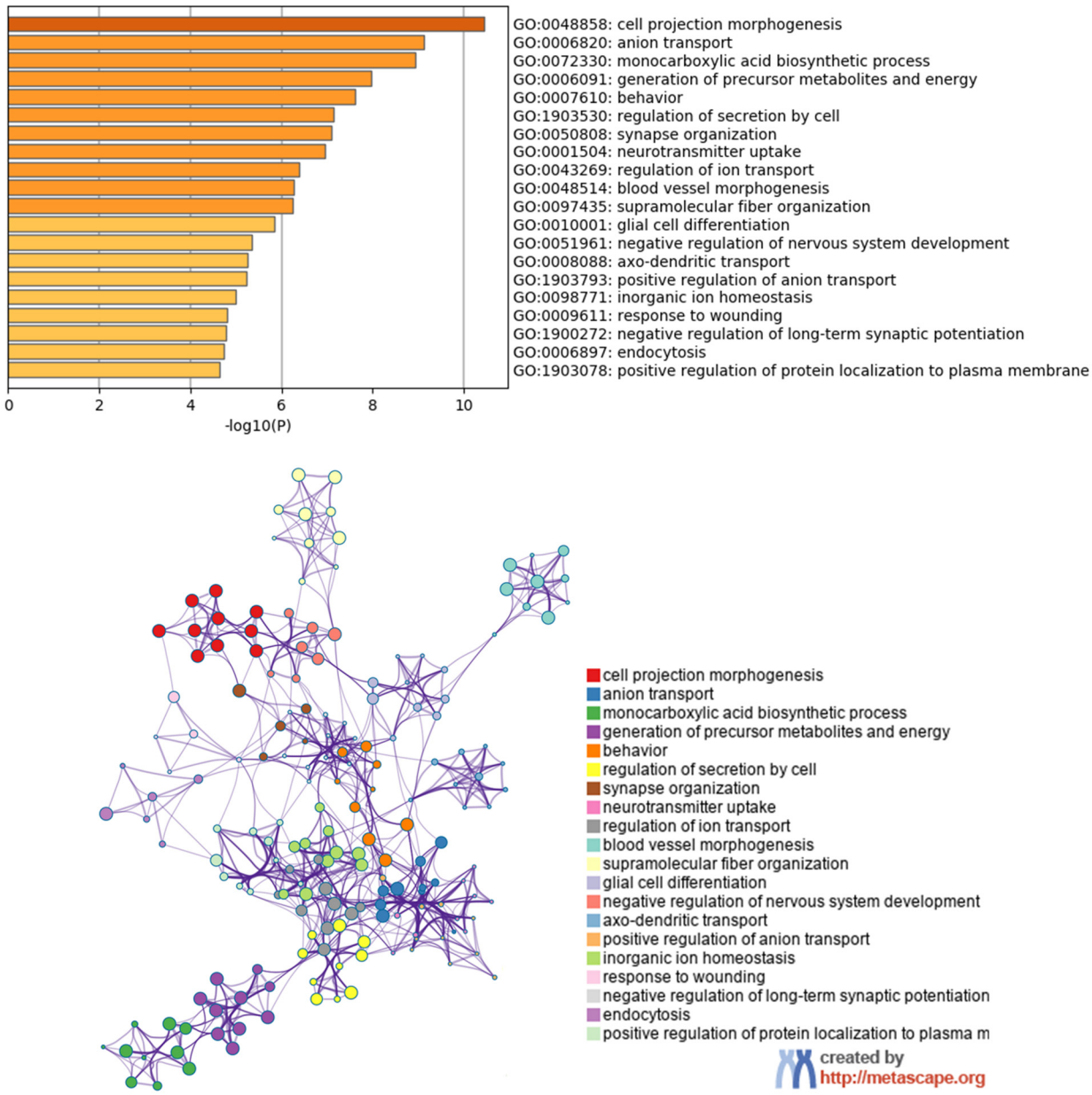

Figure S1. GO Biological processes enriched among the top 200 expressed genes in NAc astrocytes are highly interconnected. Metascape Gene Ontology (GO) Biological Process analysis of the top 200 expressed genes in NAc astrocytes reveals key metabolic and synaptic neurotransmission functions to be enriched, all processes generally attributed to astrocytes. Enrichment network analysis also revealed these top biological processes exhibit a high degree of interconnectivity.

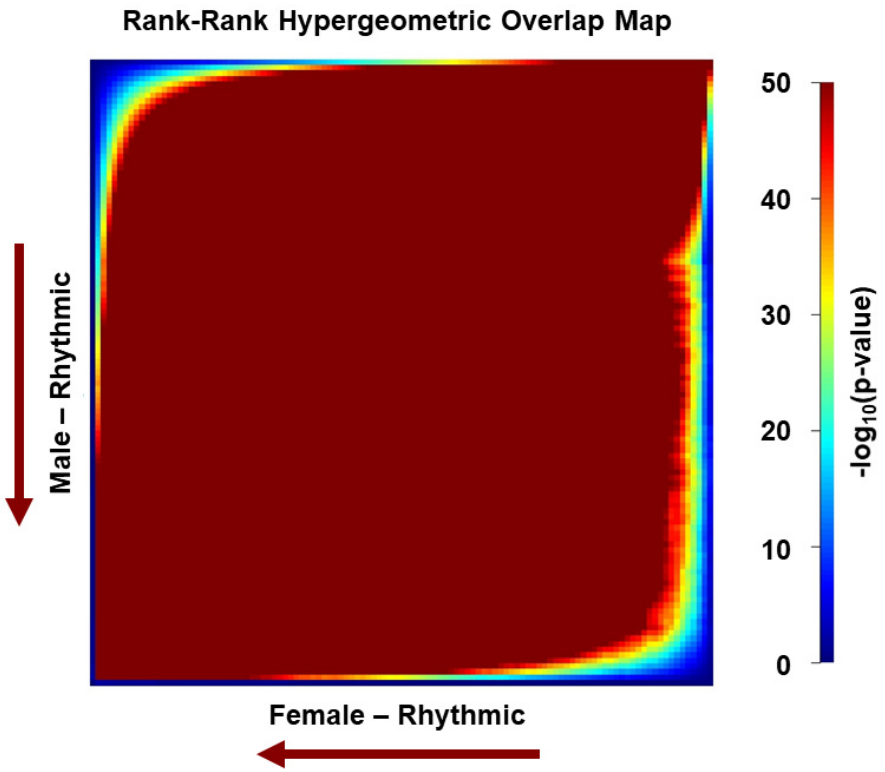

Figure S2. Male and Female mice share a high degree of overlap between NAc astrocyte-specific rhythmic transcripts identified in JTK_Cyle RNA-seq analysis. The Rank-Rank Hypergeometric Overlap (RRHO) analyis was used to determine degree of rhythmic overlap between males and females in our NAc astrocyte-specific JTK_Cycle RNA sequencing analysis. RRHO is a threshold-free approach that avoids arbitrary thresholds used in conventional venn diagram assessment (13, 14). Rhythmic genes between males and females were ranked by their -log10(p-value). RRHO plot above indicates high degree of overlap of rhythmic transcripts between male and female NAc astrocytes.

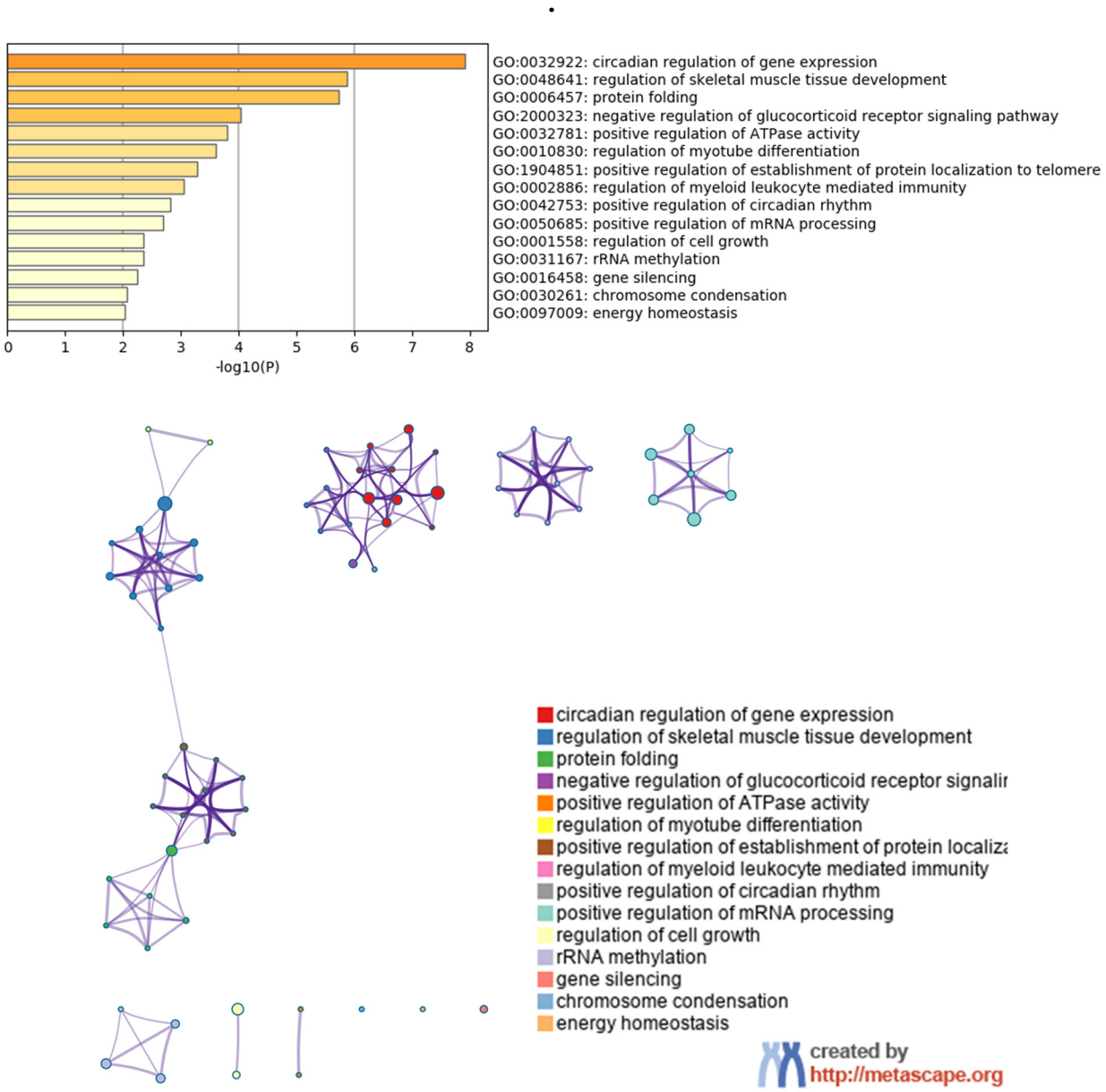

Figure S3. GO Biological processes enriched among the top 200 rhythmic genes in NAc astrocytes. Metascape Gene Ontology (GO) Biological Process analysis revealed both circadian and metabolic-related processes enriched among the top rhythmic genes identified in JTK_Cycle. Enrichment network analysis also revealed the *circadian regulation of gene expression* and *glucocorticoid receptor signaling* node clusters show a high degree of interconnectivity.

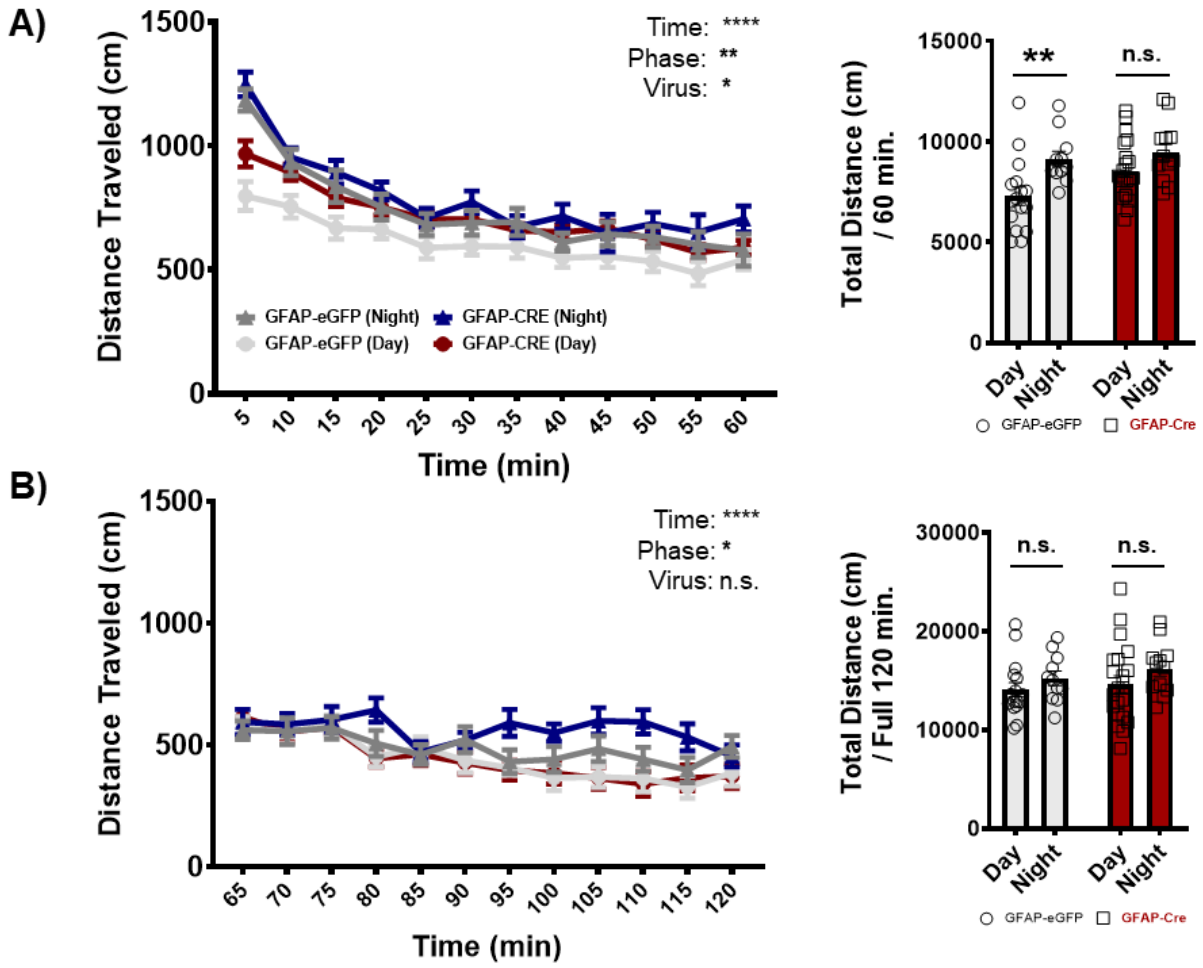

Figure S4. Loss of BMAL1 function in NAc astrocytes disrupts diurnal variation in locomotor response to novelty in mice. (**A**) In the locomotor motor response to novelty (LRN) task, eGFP control mice show diurnal variation in locomotor response to novelty, with higher locomotor response at night relative to the day. This diurnal variation is abolished following loss of BMAL1 function in NAc astrocytes (GFAP-Cre) by an increase during the day. (**B**) Loss of BMAL1 function in NAc astrocytes does not significantly alter habituation at either time of day, as measured by activity in the second hour of the 2-hour task (left), nor does it affect total locomotor activity across the full task (right). ZT0 = 7am. Day (ZT 2-6). Night (ZT 14-18). Mean ± SEM; n=12-22; * $p<0.05$, ** $p<0.01$, ****$p<0.0001$, n.s. = not significant.

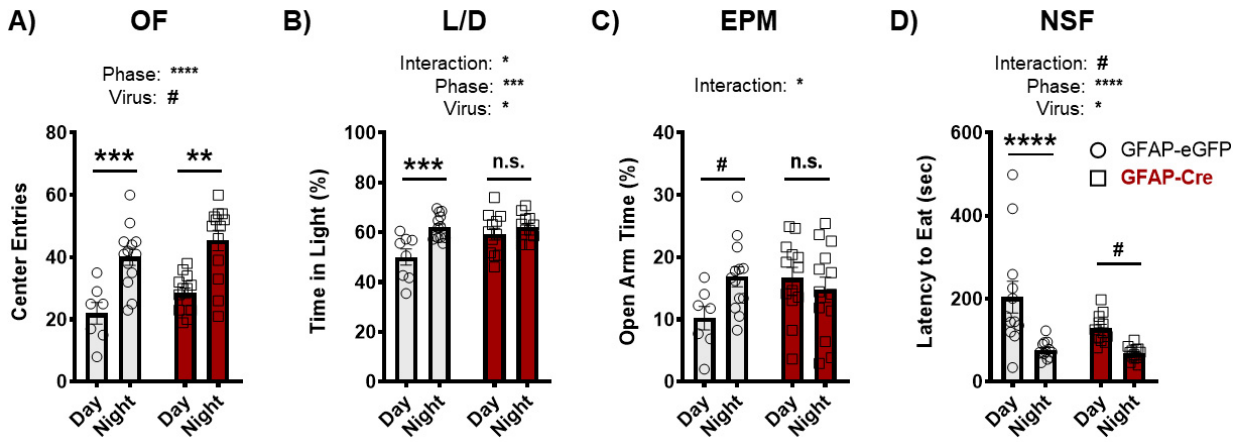

Figure S5. Loss of BMAL1 function in NAc astrocytes alters diurnal variation in exploratory drive in mice. Mice were run through a panel of behavioral assays testing exploratory drive during the day or at night. (**A**) In the open field (OF) task, both eGFP and GFAP-Cre mice show a diurnal variation in number of center entries, with greater center entries during the night. eGFP control mice show a more significant diurnal variation, relative to GFAP-Cre mice. (**B**) In the light-dark box test (L/D), eGFP mice show a significant diurnal variation in percentage of time in the brightly lit chamber of the arena, but this diurnal variation is abolished in GFAP-Cre mice. (**C**) This is also true in the elevated plus maze (EPM) task, whereby eGFP control mice show diurnal variation in open arms entries, but GFAP-Cre mice do not. (**D**) Following an overnight food restriction, eGFP mice show a significant diurnal variation in the novelty suppressed feeding (NSF) task, with a shorter latency to eat food during the night. This effect is attenuated in the GFAP-Cre mice, with an interaction *and both* main effects of phase and virus. ZT0 = 7am. Day (ZT 2-6). Night (ZT 14-18). Mean ± SEM; n=7-13; # $p \leq 0.07$, * $p < 0.05$, ** $p < 0.01$, *** $p < 0.001$, **** $p < 0.0001$.

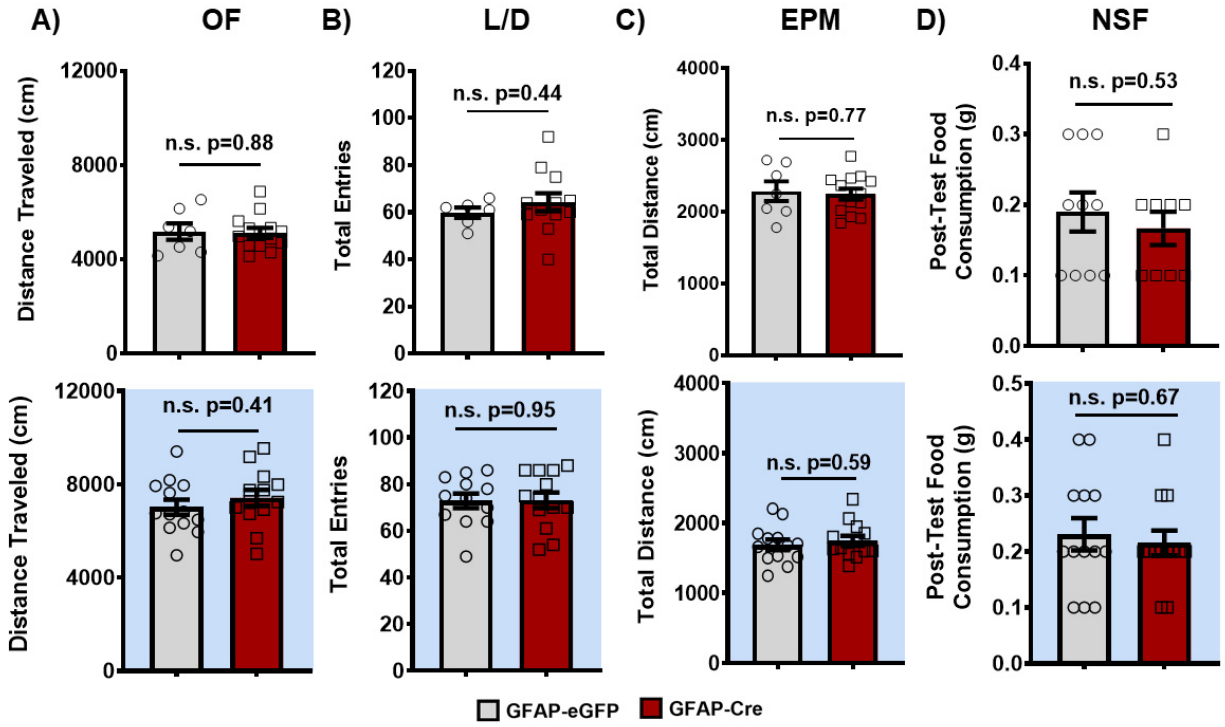

Figure S6. Increases in exploratory drive are <u>not</u> attributed to differences in locomotor activity or drive to eat.

Given that GFAP-Cre mice show a significant increase in LRN, it was important also to measure activity during the exploratory drive behavioral assays to ensure any differences seen are not being driven by locomotor differences. (**A**) Neither during the day (top) nor at night (bottom), GFAP-Cre mice show no differences in locomotor activity during the OF test, (**B)** no differences in total number of entries in the L/D test, (**C**) and no differences in l*ocomotor* activity during the EPM task. (**D**) Given that mice are food restricted overnight before the NSF task, it was important also to measure post-test food consumption to ensure any differences in latency to eat are not be*ing dr*iven by the mouse's drive/motivation to eat. In the home-cage post-test food consumpti*on assessmen*t, GFAP-Cre mice show no differences in grams of food consumed relative to control mice – suggesting the decreased latency to eat is not attributed to differences in hunger/motivation to eat. White background indicates behavior run during the day (ZT 2-6). B*lue backgrou*nd indicates behavior run during the night (ZT 14-18). Mean ± SEM; n=7-13; n.s. = not significant.

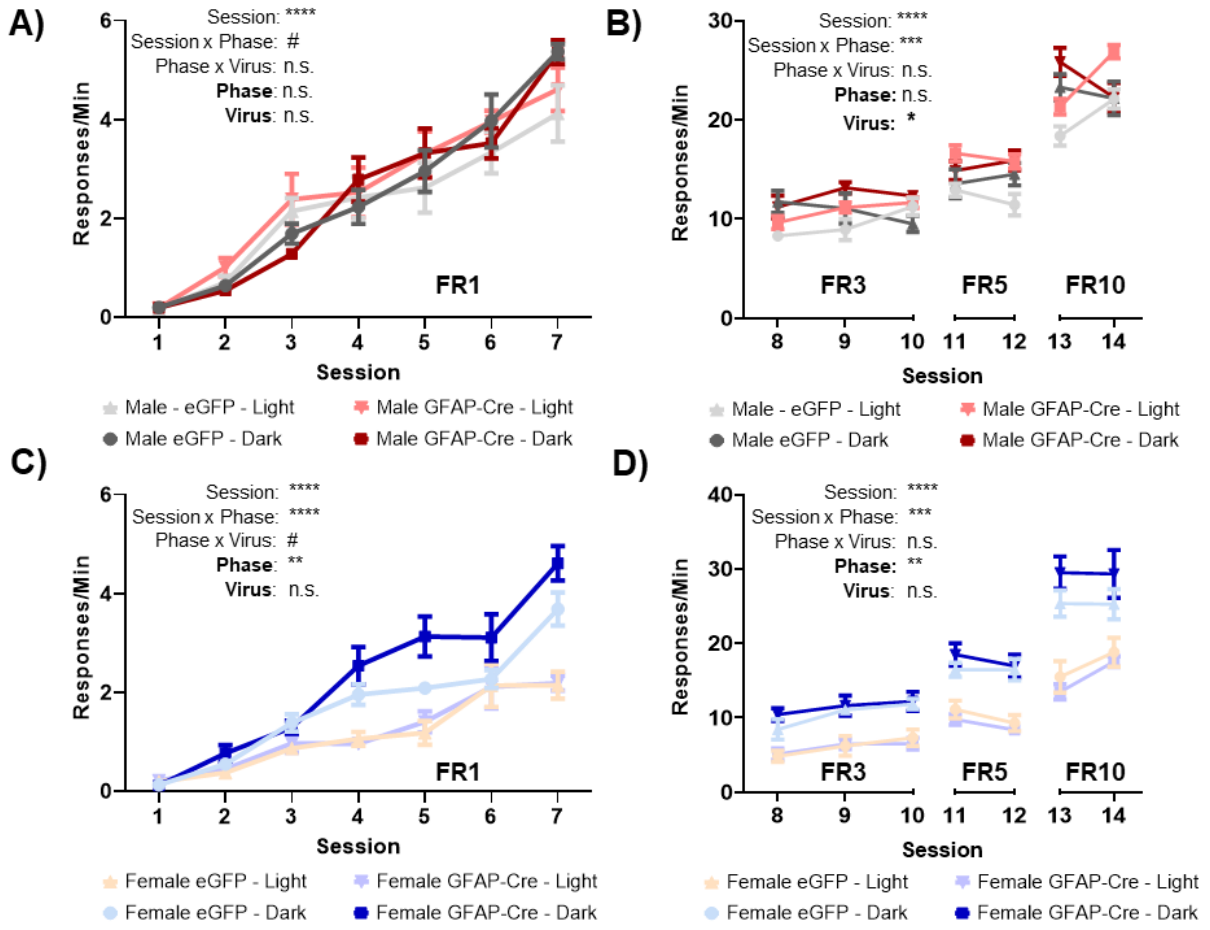

Figure S7. Loss of BMAL1 function in NAc astrocytes differentialy affects operant food self-administration in a phase- and sex-specific manner. To assess natural reward and reward-motivation, mice were trained to self-administer food pellets in an operant food self-administration task both during the day or at night. (**A**) On an FR1 schedule (i.e., 1 lever press : 1 pellet), both male eGFP and BMFL-GFAP-Cre mice successfully learn to self-administer food, but show no diurnal variation in responding. (**B**) To test reward motivation, mice were tested across increasingly difficult FR schedules (i.e., FR3, 3 presses : 1 pellet; FR5, 5 presses : 1 pellet; FR10, 10 presses : 1 pellet). *While GFAP-Cre* male mice show a robust maintenance and significant increase in food self-administration rate across FR schedules during the day, no effect was seen at night and no diurnal variation in motivation was seen. (**C**) In females, both eGFP and BMFL-GFAP-Cre mice also successfully learn to self-administer food, but actually show a significant diurnal variation in responding that is further enhanced in GFAP-Cre mice. (**E**) Testing motivation, both female mice also show maintenance and diurnal variation in motivation to self-administer, but no significant effect of GFAP-Cre virus. ZT0 = 7am. Day (ZT 2-6). Night (ZT 14-18). Mean ± SEM; n = 6; # p=0.07, * p<0.05, ** p<0.01, *** p<0.0001, ****p<0.0001.

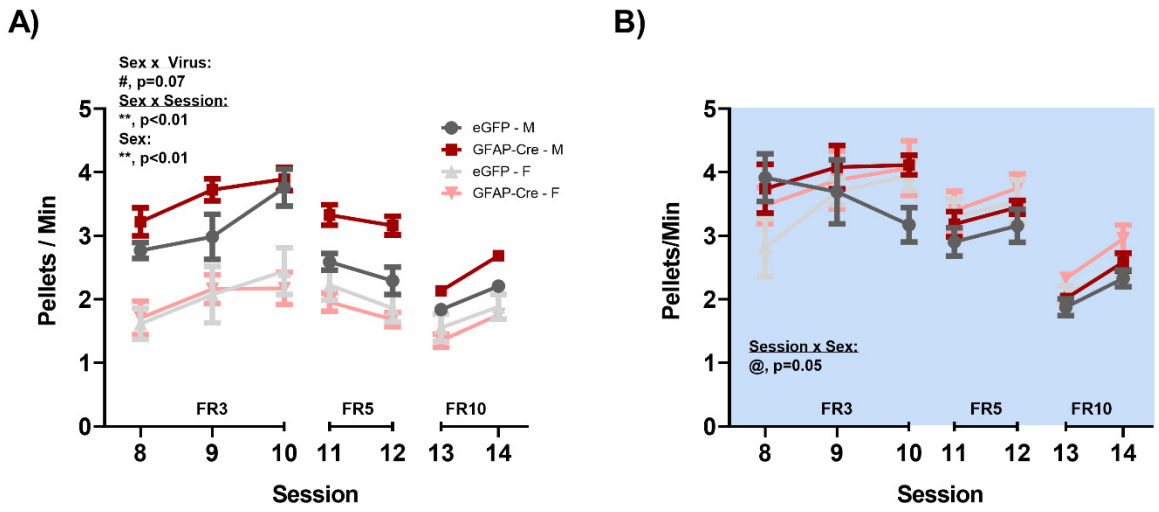

Figure S8. Loss of BMAL1 function in NAc astrocytes increases operant food self-administration pellet rate and motivation during the day. To assess natural reward and reward-motivation, both BMFL mice expressing NAc-specific GFAP-Cre or eGFP control were trained to self-administer food pellets in an operant food self-administration task both during the day and at night. (**A**) To test reward motivation, mice were tested across increasingly difficult FR schedules (i.e., FR3, 3 presses : 1 pellet; FR5, 5 presses : 1 pellet; FR10, 10 presses : 1 pellet). GFAP-Cre male mice not only show a robust maintenance of lever pressing, but also continue to increase food self-administration pellet rate across FR schedules during the day, relative to control counterparts (Sex x Virus: $F_{(1, 10)} = 3.872$, # p=0.07; Sex x Session: $F_{(3, 30)} = 6.702$, ** p=0.001; Sex: ($F_{(0.4, 4.3)} = 38.24$, ** p=0.004). (**B**) During the night, no significant differences are seen between GFAP-Cre and eGFP motivation, as tested across increasing FR schedules (Session x Sex: $F_{(3.3, 33.26)} = 2.72$, @ p=0.05). White background indicates behavior run during the day (ZT 2-6). Blue background indicates behavior run during the night (ZT 14-18). Mean ± SEM; n = 6; # p=0.07, @ p=0.05, ** p<0.01.

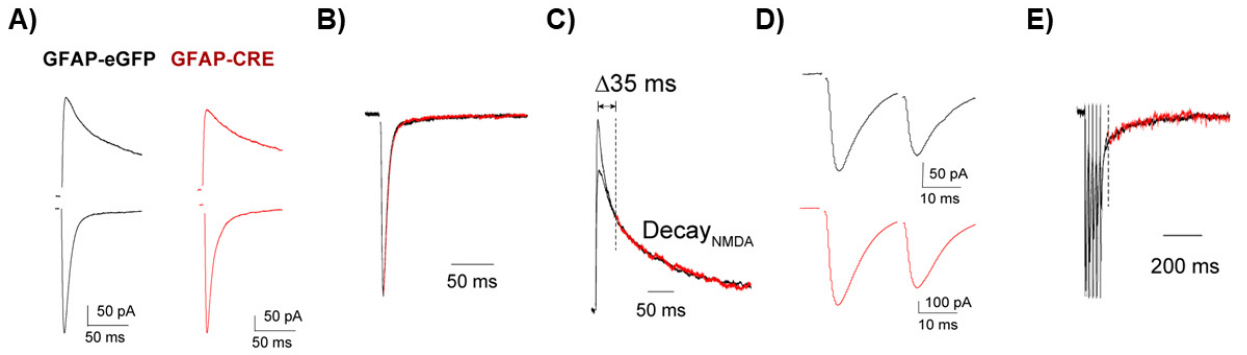

Figure S9. Loss of BMAL1 function in NAc astrocytes does not affect neighboring MSN excitatory synaptic transmission at night. Slice electrophysiology was used to assess the effects of loss of BMAL1 function in NAc astrocytes on glutamatergic signaling in neighboring MSNs during the dark phase. Representative traces showing no significant differences in (**A**) AMPA/NMDA ratio, (**B**) AMPA decay kinetics, (**C**) NMDA receptor kinetics, (**D**) paired pulse ratio (P2/PI; i.e., EPSC2/EPSC1), though trending, or (**E**) tau of the slow tail decaybetween GFAP-Cre and eGFP mice. Red traces indicate GFAP-Cre group. Recordings performed ZT16-18.

Supplemental References

1. Storch K-F, Paz C, Signorovitch J, Raviola E, Pawlyk B, Li T, *et al.* (2007): Intrinsic circadian clock of the mammalian retina: importance for retinal processing of visual information. *Cell*. 130(4): 730–741.
2. Cahoy JD, Emery B, Kaushal A, Foo LC, Zamanian JL, Christopherson KS, *et al.* (2008): A transcriptome database for astrocytes, neurons, and oligodendrocytes: a new resource for understanding brain development and function. *J. Neurosci.* 28(1): 264–278.
3. Yang Y, Vidensky S, Jin L, Jie C, Lorenzini I, Frankl M, *et al.* (2011): Molecular comparison of glt1+ and aldh1l1+ astrocytes in vivo in astroglial reporter mice. *Glia*. 59(2): 200–207.
4. Zhang Y, Chen K, Sloan SA, Bennett ML, Scholze AR, O'Keeffe S, *et al.* (2014): An rna-sequencing transcriptome and splicing database of glia, neurons, and vascular cells of the cerebral cortex. *J. Neurosci.* 34(36): 11929–11947.
5. Chandra R, Francis TC, Konkalmatt P, Amgalan A, Gancarz AM, Dietz DM, *et al.* (2015): Opposing role for egr3 in nucleus accumbens cell subtypes in cocaine action. *J. Neurosci.* 35(20): 7927–7937.
6. Sanz E, Yang L, Su T, Morris DR, McKnight GS, Amieux PS (2009): Cell-type-specific isolation of ribosome-associated mrna from complex tissues. *Proc. Natl. Acad. Sci. USA*. 106(33): 13939–13944.
7. Kim D, Paggi JM, Park C, Bennett C, Salzberg SL (2019): Graph-based genome alignment and genotyping with hisat2 and hisat-genotype. *Nat. Biotechnol.* 37(8): 907–915.
8. Anders S, Pyl PT, Huber W (2015): Htseq — a python framework to work with high-throughput sequencing data. *Bioinformatics*. 31(2): 166–169.

9. Robinson MD, McCarthy DJ, Smyth GK (2010): Edger: a bioconductor package for differential expression analysis of digital gene expression data. *Bioinformatics*. 26(1): 139–140.

10. McCarthy DJ, Chen Y, Smyth GK (2012): Differential expression analysis of multifactor rna-seq experiments with respect to biological variation. *Nucleic Acids Res.* 40(10): 4288–4297.

11. Hughes ME, Hogenesch JB, Kornacker K (2010): Jtk_cycle: an efficient nonparametric algorithm for detecting rhythmic components in genome-scale data sets. *J. Biol. Rhythms*. 25(5): 372–380.

12. Wu G, Zhu J, Yu J, Zhou L, Huang JZ, Zhang Z (2014): Evaluation of five methods for genome-wide circadian gene identification. *J. Biol. Rhythms*. 29(4): 231–242.

13. Plaisier SB, Taschereau R, Wong JA, Graeber TG (2010): Rank-rank hypergeometric overlap: identification of statistically significant overlap between gene-expression signatures. *Nucleic Acids Res.* 38(17): e169.

14. Cahill KM, Huo Z, Tseng GC, Logan RW, Seney ML (2018): Improved identification of concordant and discordant gene expression signatures using an updated rank-rank hypergeometric overlap approach. *Sci. Rep.* 8(1): 9588.

15. Krämer A, Green J, Pollard J, Tugendreich S (2014): Causal analysis approaches in ingenuity pathway analysis. *Bioinformatics*. 30(4): 523–530.

16. Zhou Y, Zhou B, Pache L, Chang M, Khodabakhshi AH, Tanaseichuk O, *et al.* (2019): Metascape provides a biologist-oriented resource for the analysis of systems-level datasets. *Nat. Commun.* 10(1): 1523.

17. Shannon P, Markiel A, Ozier O, Baliga NS, Wang JT, Ramage D, *et al.* (2003): Cytoscape: a software environment for integrated models of biomolecular interaction networks. *Genome Res.* 13(11): 2498–2504.

18. Ozburn AR, Falcon E, Twaddle A, Nugent AL, Gillman AG, Spencer SM, *et al.* (2015): Direct regulation of diurnal drd3 expression and cocaine reward by npas2. *Biol. Psychiatry*. 77(5): 425–433.

19. Lananna BV, Nadarajah CJ, Izumo M, Cedeño MR, Xiong DD, Dimitry J, *et al.* (2018): Cell-autonomous regulation of astrocyte activation by the circadian clock protein bmal1. *Cell Rep.* 25(1): 1–9.e5.

20. Tso CF, Simon T, Greenlaw AC, Puri T, Mieda M, Herzog ED (2017): Astrocytes regulate daily rhythms in the suprachiasmatic nucleus and behavior. *Curr. Biol.* 27(7): 1055–1061.

21. Caiazzo M, Giannelli S, Valente P, Lignani G, Carissimo A, Sessa A, *et al.* (2015): Direct conversion of fibroblasts into functional astrocytes by defined transcription factors. *Stem Cell Rep.* 4(1): 25–36.

22. Vargas MR, Johnson DA, Sirkis DW, Messing A, Johnson JA (2008): Nrf2 activation in astrocytes protects against neurodegeneration in mouse models of familial amyotrophic lateral sclerosis. *J. Neurosci.* 28(50): 13574–13581.

23. Chang H-C, Guarente L (2013): Sirt1 mediates central circadian control in the scn by a mechanism that decays with aging. *Cell*. 153(7): 1448–1460.

24. Nilsson LM, Forshell TZP, Rimpi S, Kreutzer C, Pretsch W, Bornkamm GW, *et al.* (2012): Mouse genetics suggests cell-context dependency for myc-regulated metabolic enzymes during tumorigenesis. *PLoS Genet.* 8(3): e1002573.

25. Schutkowski A, Wege N, Stangl GI, König B (2014): Tissue-specific expression of monocarboxylate transporters during fasting in mice. *PLoS One*. 9(11): e112118.

26. Rusnakova V, Honsa P, Dzamba D, Ståhlberg A, Kubista M, Anderova M (2013): Heterogeneity of astrocytes: from development to injury - single cell gene expression. *PLoS One*. 8(8): e69734.

27. Dzamba D, Honsa P, Valny M, Kriska J, Valihrach L, Novosadova V, *et al.* (2015): Quantitative analysis of glutamate receptors in glial cells from the cortex of gfap/egfp mice following ischemic injury: focus on nmda receptors. *Cell Mol. Neurobiol.* 35(8): 1187–1202.

28. Qin L, Williams JB, Tan T, Liu T, Cao Q, Ma K, *et al.* (2021): Deficiency of autism risk factor ash1l in prefrontal cortex induces epigenetic aberrations and seizures. *Nat. Commun.* 12(1): 6589.

29. Spandidos A, Wang X, Wang H, Seed B (2010): Primerbank: a resource of human and mouse pcr primer pairs for gene expression detection and quantification. *Nucleic Acids Res.* 38(Database issue): D792–9.

30. Zhang Y, He X, Meng X, Wu X, Tong H, Zhang X, *et al.* (2017): Regulation of glutamate transporter trafficking by nedd4-2 in a parkinson's disease model. *Cell Death Dis.* 8(2): e2574.

31. Tsujita T, Peirce V, Baird L, Matsuyama Y, Takaku M, Walsh SV, *et al.* (2014): Transcription factor nrf1 negatively regulates the cystine/glutamate transporter and lipid-metabolizing enzymes. *Mol. Cell. Biol.* 34(20): 3800–3816.

32. Schmittgen TD, Livak KJ (2008): Analyzing real-time pcr data by the comparative ct method. *Nat. Protoc.* 3(6): 1101–1108.

33. Muraleedharan R, Gawali MV, Tiwari D, Sukumaran A, Oatman N, Anderson J, *et al.* (2020): Ampk-regulated astrocytic lactate shuttle plays a non-cell-autonomous role in neuronal survival. *Cell Rep.* 32(9): 108092.

34. Baxter PS, Bell KFS, Hasel P, Kaindl AM, Fricker M, Thomson D, *et al.* (2015): Synaptic nmda receptor activity is coupled to the transcriptional control of the glutathione system. *Nat. Commun.* 6: 6761.

35. Haskew-Layton RE, Payappilly JB, Smirnova NA, Ma TC, Chan KK, Murphy TH, *et al.* (2010): Controlled enzymatic production of astrocytic hydrogen peroxide protects neurons from oxidative stress via an nrf2-independent pathway. *Proc. Natl. Acad. Sci. USA*. 107(40): 17385–17390.

36. Lerchundi R, Fernández-Moncada I, Contreras-Baeza Y, Sotelo-Hitschfeld T, Mächler P, Wyss MT, *et al.* (2015): Nh4(+) triggers the release of astrocytic lactate via mitochondrial pyruvate shunting. *Proc. Natl. Acad. Sci. USA*. 112(35): 11090–11095.

37. Parekh PK, Logan RW, Ketchesin KD, Becker-Krail D, Shelton MA, Hildebrand MA, *et al.* (2019): Cell-type-specific regulation of nucleus accumbens synaptic plasticity and cocaine reward sensitivity by the circadian protein, npas2. *J. Neurosci.* 39(24): 4657–4667.

38. Guilloux J-P, Seney M, Edgar N, Sibille E (2011): Integrated behavioral z-scoring increases the sensitivity and reliability of behavioral phenotyping in mice: relevance to emotionality and sex. *J. Neurosci. Methods*. 197(1): 21–31.